Available online at www.sciencedirect.com
SCIENCE DIRECT
Journal of Crystal Growth 289 (2006) 295–298
JOURNAL OF CRYSTAL GROWTH
www.elsevier.com/locate/jcrysgro

Formation mechanism of individual alumina nanotubes wrapping metal (Cu and Fe) nanowires

G.S. Huang[a], Y. Xie[a], X.L. Wu[a,*], L.W. Yang[a], Y. Shi[a], G.G. Siu[b], Paul K. Chu[b]

[a]National Laboratory of Solid State Microstructures and Department of Physics, Nanjing University, Nanjing 210093, People's Republic of China
[b]Department of Physics and Materials Science, City University of Hong Kong, Kowloon, Hong Kong, People's Republic of China

Received 9 August 2005; received in revised form 26 October 2005; accepted 14 November 2005
Available online 7 February 2006
Communicated by J.M. Redwing

Abstract

Using electrochemical deposition onto porous anodic alumina membrane and subsequent ultrasonic treatment, we have obtained individual alumina nanotubes wrapping metal (Cu and Fe) nanowires with nanocrystalline structure, which are a kind of conventional nanocable prototype. Scanning electron microscope and transmission electron microscope observations and X-ray diffraction, energy dispersive X-ray fluorescence, and selected area electron diffraction analyses clearly show the formation of a composite nanotube structure. Its formation mechanism is discussed on the basis of microstructural characterization. Our experiments provide a useful way for fabricating low-cost and large-scale metal nanocables, which will be of important applications in nanodevices.

PACS: 61.46.+w; 82.45.Cc; 61.10.Nz

Keywords: A1. Formation mechanism; B1. Cu/Fe nanowires; B1. Alumina nanotubes

1. Introduction

Porous anodic alumina (PAA) membrane with ordered nanopore array has attracted an increasing interest due to its simple preparation technique and favorable applications as a template in fabricating nanostructured materials [1–6]. Many kinds of materials have been filled into nanochannels of PAA membranes to fabricate different nanostructures such as Ni nanotubules [7], ZnO nanowire arrays [8], PPV nanotubes (nanorods) [9], and Eu_2O_3 nanotube arrays [10]. Of all the fabricated materials, their magnetic and luminescent properties are the subjects of many investigations. So far, little has been done in obtaining alumina nanotubes (ANTs). Recently, our research group reported formation of the ANTs from Si-based PAA membrane [5,11], which are flexible [11] and have important dielectric properties [12]. However, unruly and fussy process of fabricating Si-based PAA membrane makes it difficult to have reproducibility in obtaining the ANTs. Furthermore, short lengths of the obtained ANTs also limit their applications in requiring high aspect ratio of the nanotubes. To improve the fabrication method, we consider obtaining the ANTs from Al-based PAA membrane and expect to fabricate metal-nanowire-embedded ANTs with long lengths, which are a kind of conventional nanocable prototypes. In this letter, we firstly describe the fabrication of the ANTs from Al-based PAA membrane and then report the formation and growth mechanism of the ANTs wrapping metal (Fe and Cu) nanowires based on microstructural observations and spectral analyses. Our experiment results provide a promising way of fabricating conventional nanocables, which could be expected to have applications in modern nanoelectronics.

2. Experimental details

High-purity Al foils (99.99%) were used to fabricate the PAA membranes. The Al foil was firstly electropolished in a mixed solution of perchloric acid and ethanol (1:5 in

*Corresponding author.
E-mail address: hkxlwu@nju.edu.cn (X.L. Wu).

0022-0248/$ - see front matter © 2006 Elsevier B.V. All rights reserved.
doi:10.1016/j.jcrysgro.2005.11.124

volume) under a constant DC voltage of 18 V for 3 min. Anodization was conducted in 0.5 M oxalic acid under a DC voltage of 40 V. The electrolyte was maintained at 5 °C and mechanically stirred. Two-step anodic process was adopted to obtain high qualitative PAA membrane [13], in which anodic times were set for 3 and 2.5 h, respectively. The obtained PAA membrane was dipped into a solution of 6 wt% H_3PO_4 to enlarge the nanopores and thin the barrier layer at the bottoms of nanopores. Since Fe and Cu have large difference in electrodeposition, we explored a series of experimental conditions and then selected Fe electrodeposition to be performed in an acidic solution of 0.5 M $FeSO_4$ and 0.5 M H_3BO_3 under a constant DC voltage of 20 V and Cu electrodeposition in a solution of 0.9 M $CuSO_4$ and 0.45 M H_2SO_4 under 18 V. We found that the use of proper DC voltage is crucial in metal electrodeposition, which ensures that metal nanowires can be deposited into nanochannels rather than onto the surface of the PAA membrane. Since partial voltage drops across the barrier layer, the applied voltage is higher in our experiments than that in common eletrodeposition [14]. After electrochemical deposition, surplus Al substrate was removed using a saturated $CuCl_2$ aqueous solution. The freestanding membrane was then immersed into 0.1 M NaOH solution to dissolve partial alumina. The resulting membrane was subjected to ultrasonic vibration in de-ionized water for 20 s and the separated fragments were finally fished out with Cu grid to carry out transmission electron microscope (TEM) observations. The microstructure and chemical compositions of the sample were characterized using a DI nanoscope IIIa Atomic force microscope (AFM), a LEO 1530VP scanning electron microscope (SEM) equipped with an EDAX PV7715/89 ME energy dispersive X-ray fluorescence (EDXF) spectrometry, and a JEOL JEM-200CX TEM. X-ray diffraction (XRD) patterns were obtained on an X-ray rotating-anode diffractometer (D/max-rA, Rigaku) with Cu $K\alpha$ radiation. All the measurements were carried out at room temperature.

3. Results and discussion

Fig. 1(a) shows the AFM image of the as-anodized PAA membrane with a thickness of $>4\,\mu m$. A perfectly ordered nanopore array can clearly be observed. The array shows a density-packed hexagonal structure with an average nanopore diameter of ~50 nm and interpore distance of ~110 nm. A circular protrusion occurs at each corner of the hexagonal cell. The thicknesses of the pore walls are inhomogeneous and the thinnest locations are at the centers between two neighboring protrusions. This is a key condition for the formation of individual ANTs. With subsequent ultrasonic vibration, thin boundaries (the thinnest locations) of some cells will be broken. If six neighboring pore walls connected with a cell are broken, an individual ANT will be formed (see the circle in Fig. 1(a)). This cleavage fashion can easily be seen during our TEM observation. Furthermore, we found that excessive ultrasonic vibration will cause large ruin of the ANTs. On the contrary, insufficient ultrasonic vibration will lead to incomplete detachment of the ANTs, as shown in Fig. 1(b), which displays a row of incompletely detached ANTs with some broken tube walls (by the arrow). Thus, adequate ultrasonic vibration is the most crucial condition for fabricating individual ANTs. In our current experiments, an ultrasonic vibration of 20 s was found to be the best parameter for the ANT fabrication because it always leads to the formation of numerous individual ANTs from run to run. However, for different PAA membranes, the ultrasonic vibration duration is different. For example, for the PAA membrane with a thickness of $>1.5\,\mu m$ and a pore diameter of 80 nm, the ultrasonic vibration duration should be taken less than 10 s so as to obtain the perfect ANTs [15]. Otherwise large ruin of the ANTs will take place. For the PAA membrane with a thickness of $<0.5\,\mu m$, even an ultrasonic vibration is not necessary for obtaining the ANTs [16]. Here we should stress that our deduction to the formation mechanism of the ANTs is also based on the observation of some alumina nanowires (ANWs) and broken ANTs (see Figs. 2(a) and (b), which are produced by breaking three neighboring pore walls connected to a central protrusion. A perfect ANT with inner diameter of ~80 nm and length of $>4\,\mu m$ is shown in Fig. 1(c). Its tube-like morphology does not change with tilting the sample holder during our TEM observations. Some residual tube walls can also be observed clearly (by

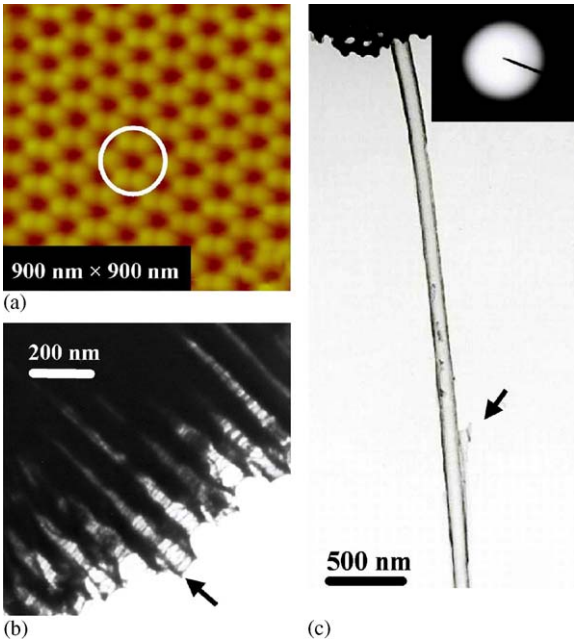

Fig. 1. (a) AFM image of the obtained PAA membrane. The circle demonstrates a cell possibly forming an individual ANT. (b) TEM image of a row of incompletely detached ANTs from Al-based PAA membrane. The arrow shows the broken tube wall. (c) TEM image of a perfect ANT with some resident tube walls. Its inset presents the SAED pattern of the ANT.

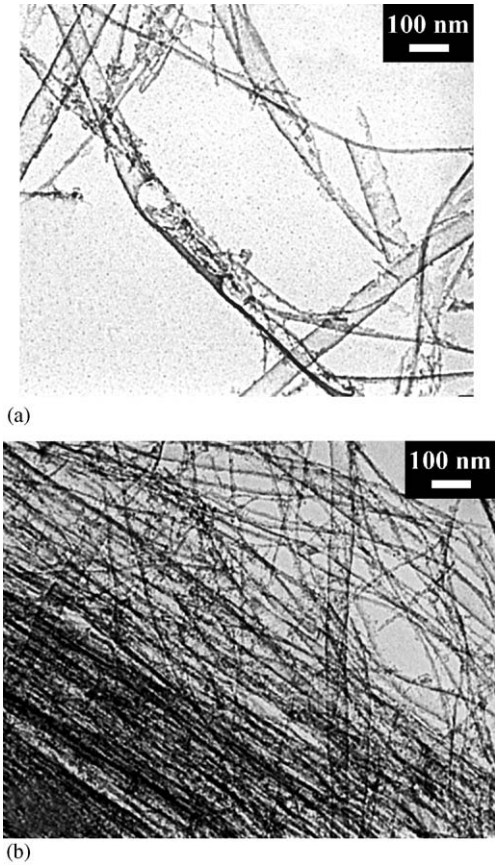

Fig. 2. (a) TEM image of some broken ANTs and ANWs. (b) TEM image of a bundle of individual ANWs.

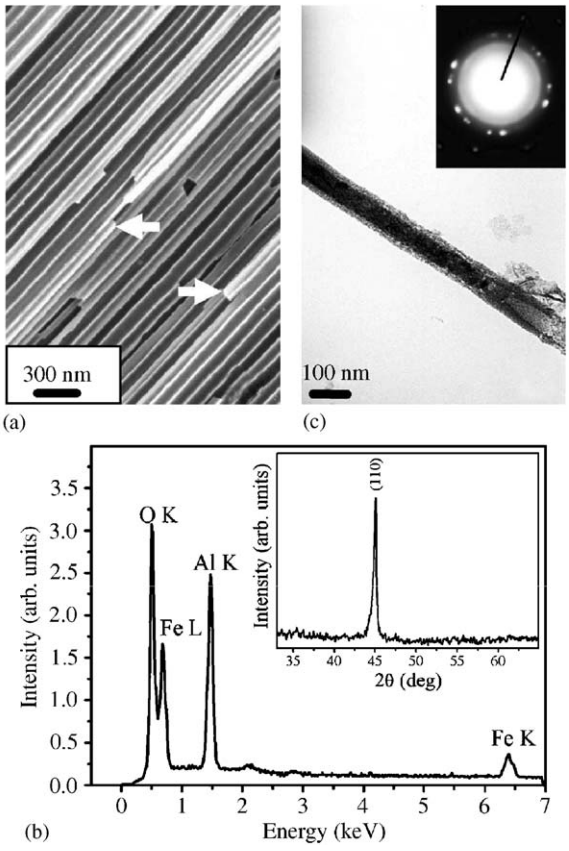

Fig. 3. (a) Cross-sectional SEM image of Fe-deposited PAA membrane. The arrows show Fe nanowires in the white. (b) EDXF spectrum of Fe-deposited PAA membrane. Its inset illustrates the corresponding XRD spectrum. (c) TEM image of an ANT wrapping Fe nanowire. Its inset displays the corresponding SAED pattern.

the arrow). The inset of Fig. 1(c) presents the corresponding selected area electron diffraction (SAED) pattern. A broad halo spot reflects amorphous structure of the ANT. This is consistent with previous XRD result [17]. The $>4\,\mu m$ length of the obtained ANT is far longer than several-hundred nanometer length of the ANT from Si-based PAA membrane. Due to chemical etching in dilute H_3PO_4 and NaOH solutions, the inner diameter of the ANT is larger than that of nanopore in the as-anodized PAA membrane. Generally, we may infer from the formation mechanism that intact ANTs and ANWs should occupy only a small proportion relative to total products (intact ANTs, ANWs, broken ANTs, and remaining PAA segments) from our TEM observations. The amounts are estimated to be ~10% for the ANTs and ~30% for the ANWs. However, high nanopore density of the PAA membrane will make total throughput of perfect ANT still very large under adequate ultrasonic treatment. Therefore, numerous intact ANTs, similar to those shown in Fig. 1(b), can be obtained. This indicates that the current fabrication method is effective in obtaining large-scale ANTs from Al-based PAA membrane.

Fig. 3(a) shows the cross-sectional SEM image of Fe-deposited PAA membrane. Though some Fe nanowires in nanochannels have been lost during sample preparation, some white nanowires marked by the arrows can still be seen. The EDXF spectrum of this nanowire is presented in Fig. 3(b). The existence of Fe L and K peaks clearly indicates that Fe nanowires have been deposited into nanochannels. Al and O peaks in the spectrum are from the PAA membrane. The inset of Fig. 3(b) illustrates the XRD spectrum of Fe-deposited PAA membrane. The (1 1 0) diffraction peak with a lattice constant of $a = 0.2866\,nm$ is very strong and perfectly matches with bcc structure of Fe. Fig. 3(c) displays the TEM image of an ANT wrapping Fe nanowire with a diameter of ~63 nm. The SAED pattern of this composite nanotube structure clearly shows some diffraction spots from Fe (1 1 0) plane (see the inset of Fig. 3(c). Fig. 4(a) shows the XRD spectrum of Cu-deposited PAA membrane. The (1 1 1) and (3 3 1) diffraction peaks are from Cu nanowires embedded in nanochannels. The deposition of Cu inside the ANTs is confirmed by our TEM observations (see Fig. 4(b), which shows a Cu nanowire embedded in an ANT). The corresponding SAED pattern clearly exhibits some diffraction spots from Cu (1 1 1) planes (see the inset), indicating that the deposited Cu nanowires are of crystalline structure. Here, we should point out that the wall thicknesses of the ANTs

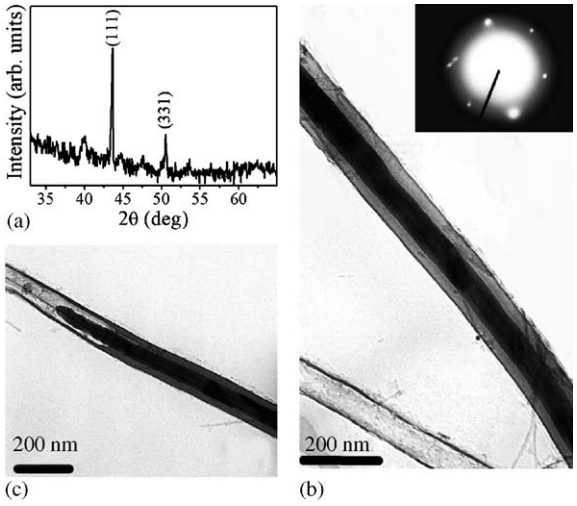

Fig. 4. (a) XRD spectrum of Cu-deposited PAA membrane. (b) TEM image of two ANTs wrapping and unwrapping Cu nanowires, respectively. Its inset exhibits the SAED pattern of the ANT wrapping Cu nanowire. (c) TEM image of an ANT half-filled with Cu nanowire.

before and after wrapping metal nanowire are very different (a hollow ANT is also shown in Fig. 4(b)). This phenomenon may be attributed to the existence of metal nanowires in nanochannels of the PAA membrane, which protects the tube walls from lateral etching in NaOH solution. This attribution can be verified in Fig. 4(c), which clearly shows a difference between wrapping and unwrapping parts of an ANT. The thickness of the tube wall obviously changes with the filling status. Finally, we would like to mention that in our experiments, we found that more than a half of the obtained individual ANTs have wrapped metal nanowires in electrochemically deposited sample, which means that the current fabrication method is effective in obtaining individual conventional nanocables.

4. Conclusion

We have obtained individual ANTs from Al-based PAA membrane and the ANTs wrapping Fe/Cu nanowires with crystalline structure using electrochemical deposition and ultrasonic vibration. The fabrication condition and formation mechanism of the ANTs are discussed on the basis of microstructural characterization. Our experiment results provide an effective way for fabricating low cost and large-scale conventional nanocables, which will be useful in nanodevices. To benefit future practical applications, more work is needed to further improve the fabrication conditions.

Acknowledgement

This work was supported by the National Natural Science Foundation of China (Nos. 10225416 and 60421003) and the LAPEM. Partial support was also from the Major State Basic Research Project No. G001CB3095 of China and Hong Kong Research Grants Council (RGC) Competitive Earmarked Research Grants (CERG) #CityU 1137/03E and CityU 1120/04E, and City University of Hong Kong Strategic Research Grant (SRG) #7001642.

References

[1] Y. Yamamoto, N. Baba, S. Tajima, Nature (London) 289 (1981) 572.
[2] R.C. Furneaux, W.R. Rigby, A.P. Davidson, Nature 337 (1989) 147.
[3] H. Masuda, K. Fukuda, Science 268 (1995) 1466.
[4] A.P. Li, F. Müller, A. Birner, K. Nielsch, U. Gösele, J. Appl. Phys. 84 (1998) 6023.
[5] L. Pu, X.M. Bao, J.P. Zou, D. Feng, Angew. Chem. Int. Edn. 113 (2001) 1538.
[6] K.L. Hobbs, P.R. Larson, G.D. Lian, J.C. Keay, M.B. Johnson, Nano Lett. 4 (2004) 167.
[7] J.C. Bao, C.Y. Tie, Z. Xu, Q.F. Zhou, D. Shen, Q. Ma, Adv. Mater. 13 (2001) 1631.
[8] C.H. Liu, J.A. Zapien, Y. Yao, X.M. Meng, C.S. Lee, S.S. Fan, Y. Lifshitz, S.T. Lee, Adv. Mater. 15 (2003) 838.
[9] K.K. Kim, J.I. Jin, Nano Lett. 1 (2001) 631.
[10] G.S. Wu, L.D. Zhang, B.C. Cheng, T. Xie, X.Y. Yuan, J. Am. Chem. Soc. 126 (2004) 5976.
[11] Y.F. Mei, X.L. Wu, X.F. Shao, G.G. Siu, X.M. Bao, Europhys. Lett. 62 (2003) 595.
[12] H.J. de Wit, C. Wijenberg, C. Crevecoeur, J. Electrochem. Soc. 123 (1976) 1479.
[13] H. Masuda, M. Satoh, Jpn. J. Appl. Phys. Part 2 35 (1996) L126.
[14] M.E. Toimil Molares, V. Buschmann, D. Dobrev, R. Neumann, R. Scholz, I.U. Schuchert, J. Vetter, Adv. Mater. 13 (2001) 62.
[15] X.F. Shao, X.L. Wu, G.S. Huang, T. Qiu, M. Jiang, J.M. Hong, Appl. Phys. A 81 (2005) 621.
[16] Y.F. Mei, X.L. Wu, X.F. Shao, G.S. Huang, G.G. Siu, Phys. Lett. A 309 (2003) 109.
[17] G.S. Huang, X.L. Wu, Y. Xie, X.F. Shao, S.H. Wang, J. Appl. Phys. 94 (2003) 2407.